Strain splitting of nitrogen acceptor levels in ZnSe

H. Mayer and U. Rössler
Institut für Theoretische Physik, Universität Regensburg, D-93040 Regensburg, Germany

K. Wolf, A. Elstner, H. Stanzl, T. Reisinger, and W. Gebhardt
Institut für Festkörperphysik, Universität Regensburg, D-93040 Regensburg, Germany
(Received 29 November 1994)

We report on the experimental and theoretical study of the strain splitting of nitrogen acceptor levels in epitaxially grown ZnSe on GaAs substrate. The crystal strain is due to the different lattice constants and thermal expansion coefficients and is determined by x-ray diffractometry. The binding energies of the acceptor ground and excited states have been determined by temperature-dependent and resonant photoluminescence measurements involving two-hole transitions for three differently strained layers. A consistent theoretical description of the experimental data is given in terms of the model of Baldereschi and Lipari, augmented by the Bir-Pikus Hamiltonian to account for the strain splitting of the valence-band edge. An empirical ansatz for the central-cell correction is used in order to reproduce the chemical shift of the nitrogen acceptor.

I. INTRODUCTION

The great interest in wide-gap II-VI semiconductors is due to their potential use in optoelectronic devices operating in the blue spectral region.[1,2] The recent success in demonstrating a blue-green laser diode is based on the progress in growing low-resistivity p-type ZnSe using nitrogen as a dopant. For the fabrication of such crystals, molecular beam epitaxy (MBE) or metalorganic vapor phase epitaxy (MOVPE) techniques are employed. Usually the crystals are grown by heteroepitaxy, thus leading to biaxially strained layers due to the combined effect of lattice mismatch and different thermal expansion coefficients of layer and substrate. Therefore, the characterization of the grown II-VI material is mostly performed on strained epitaxial layers, and any detailed analysis of the spectra has to account for the crystal strain. It is the purpose of the present paper to report on the systematic investigation of the strain splitting of the $1S_{3/2}$ acceptor ground state and the $2S_{3/2}$ excited state in a II-VI semiconductor. Different strain values are realized in layers of different thicknesses. The strength of the strain is determined by x-ray diffractometry. Unstrained layers are prepared by removing the substrate.

The concept to describe shallow bound acceptor states within the framework of $\mathbf{k}\cdot\mathbf{p}$ theory is due to Luttinger and Kohn,[3] a meaningful classification of the acceptor states has been given by Baldereschi and Lipari.[4] This treatment of the acceptor problem opens the possibility for a direct relation between details of the valence-band structure and spectral data obtained from shallow acceptor states. Within the $\mathbf{k}\cdot\mathbf{p}$ approach, hole states bound to the acceptor by Coulomb interaction are considered as wave packets of valence-band states from the vicinity of the band edge. Due to the fourfold degeneracy of the valence-band edge, the kinetic energy term of the acceptor problem contains a coupling between hole quasispin ($J = 3/2$) and angular momentum. The resulting fine-structure splitting of the bound states provides detailed information about the band structure, which can be exploited to determine the valence-band Luttinger parameters.

In the past, the $\mathbf{k}\cdot\mathbf{p}$ method has been extended to consider crystal strain and applied successfully to interpret experimental data for acceptors in group IV semiconductors and III-V compounds.[5,6] The Hamiltonian, which describes the influence of the crystal strain on the valence-band structure and, hence, on the acceptor spectra, has been formulated by Bir and Pikus.[7]

The chemical nature of the impurity exhibits itself in a central-cell correction,[8] which affects primarily the acceptor ground state and has only negligible effect on states with odd parity. We employ a phenomenological model to account for the chemical shift,[9] containing a single parameter that is fitted to the acceptor ground-state energy in the unstrained crystal. A consistent quantitative explanation of additional spectral data, including their strain dependence, justifies this concept.

II. SAMPLE PREPARATION

All investigated epilayers were synthesized in our laboratory by MOVPE and MBE. GaAs (001) was used as the substrate material. The morphology of the layers was controlled by Normarski interference microscopy and the thickness was determined by interference patterns and ellipsometric measurements.

For the MOVPE process, dimethylzinc-triethylamine (DMZn-TEN), di-tertiary-butylselenide (DTBSe), and triallylamine (TAN) were used as metalorganic precursors. The GaAs substrates were prepared in a standard degrease, etched for 1 min in concentrated H_2SO_4 and finally preheated 15 min at 400 °C in a H_2 atmosphere

0163-1829/95/52(7)/4956(9)/$06.00

prior to the layer growth in the reactor. A growth rate of about 1 μm per hour was obtained at a susceptor temperature of 340 °C and an input partial pressure ratio (VI/II) of 3. Further details of the MOVPE growth process have been published elsewhere.[10,11]

For the MBE growth, we used a conventional high vacuum chamber with Knudsen cells at a growth temperature of approximately 300 °C. The GaAs substrates were prepared with a similar chemical etching procedure as that for MOVPE growth. Prior to the growth, the substrates were treated with a H plasma inside the MBE chamber, which leads to oxide free and sharp interfaces. The H plasma is produced in a rf-plasma source, which is also used for p-doping of ZnSe with nitrogen.[12] For all MBE grown samples, a two-dimensional growth mode was recorded by a reflection-high-energy-electron diffraction system.

Strain-free ZnSe layers were achieved by removing the GaAs substrate by chemical polishing and successive chemical etching.[13]

III. EXPERIMENTAL DETAILS

The structural quality and the strain of the epitaxial layers at room temperature were investigated with a Philips high-resolution x-ray diffractometer. The x-rays originating from a Cu tube were monochromated by the four reflections of a Bartels monochromator[14] at the (220) and ($\bar{2}\bar{2}0$) faces of two perfect channel-cut germanium single crystals. The samples were mounted on a computer controlled sample holder and a xenon proportional counting system was used as detector.

In order to determine the strain of the layer material, it is necessary to perform x-ray diffraction measurements for different asymmetrical reflections like (224) and ($\bar{2}\bar{2}4$). The strain of the layers can be calculated from the angular difference between the substrate and the layer peak as described in Refs. 14 and 15.

For the epitaxial system ZnSe/GaAs, the lattice mismatch

$$f = \frac{a_{\mathrm{GaAs}} - a_{\mathrm{ZnSe}}}{a_{\mathrm{ZnSe}}} \tag{1}$$

at the growth temperature of about 350 °C is $f = -0.31\%$. This lattice mismatch causes a strain in the layer material, whereas the substrate remains unstrained. At the so-called critical thickness [220 ± 20 nm for the system ZnSe/GaAs (Ref. 16)] the strain starts to relax by the nucleation of misfit dislocations during growth.[15,16] The exact value of the critical thickness depends on the growth conditions.[16] The strain of the layers at room temperature (RT) or at 2 K

$$\epsilon_{\mathrm{biax}} = \epsilon_{\mathrm{res}} + \epsilon_{\mathrm{therm}} \tag{2}$$

is caused by the residual strain at growth temperature ϵ_{res} and the thermal strain[17] $\epsilon_{\mathrm{therm}}$, which is due to different thermal expansion coefficients of ZnSe and GaAs [$\epsilon_{\mathrm{therm}}(350\,^{\circ}\mathrm{C} \rightarrow 20\,^{\circ}\mathrm{C}) = +0.04\%$; $\epsilon_{\mathrm{therm}}(350\,^{\circ}\mathrm{C} \rightarrow 2\ \mathrm{K}) = +0.1\%$]. For layers that are thinner than the critical thickness, the strain at growth temperature is determined by the lattice mismatch of substrate and layer material ($\epsilon_{\mathrm{res}} = -0.31\%$). Therefore, a constant strain of $\epsilon_{\mathrm{biax}} = -0.27\%$ is observed at RT and $\epsilon_{\mathrm{biax}} = -0.21\,\%$ at 2 K, respectively. At a thickness of 0.5 μm, the strain is largely reduced, 1-μm-thick layers are unstrained at RT.[16]

Photoluminescence (PL) measurements were performed in a liquid-helium bath cryostat (2 K) or in a temperature variable cryostat (2 K – RT) using the UV lines of an argon-ion laser (excitation energy $\approx$ 3.5 eV). The luminescence light was analyzed with a 1-m Jarrol-Ash double monochromator, which is equipped with two gratings of 1200 lines per mm and detected with a cooled GaAs photomultiplier cathode. A cw-dye laser operating with Stilben 3 and pumped with the UV lines of a 20-W argon-ion laser allowed a continuous variation of the excitation wavelength selected by a birefringent filter.

For temperatures above 20 K, donors are largely ionized and transitions of electrons from the conduction band to the acceptor ground state can be observed in PL spectra. Therefore, a systematic analysis of temperature-dependent PL measurements allows us to determine the binding energy of the acceptor ground state. Investigations of excited acceptor states have to be performed by resonant PL methods. Resonant excitation of acceptors results in luminescence processes and a strong enhancement of two-hole transitions (THT's) as well as of selective pair luminescence (SPL).

The optical process of a THT can be schematically described in the following way:

$$\gamma + A \rightarrow (A, X) \rightarrow A^* + \gamma', \tag{3}$$

with

$$h\nu - h\nu' = E_{A^*} - E_A\ . \tag{4}$$

This scheme describes the inelastic scattering of an incoming photon γ with energy $h\nu$ at a neutral acceptor A, which is left in an excited state A^*. The scattered photon γ' has energy $h\nu'$, (A, X) denotes the intermediate state of an exciton bound to a neutral acceptor and can be used for resonance enhancement of the THT process.

For the observation of SPL, donor-acceptor-pair (DAP) transitions are induced. Therefore, a sufficient amount of donors and acceptors has to be incorporated in the investigated sample. In a first step, transitions from excited acceptor states E_{A^*} to donor ground states E_D are induced (E_0: gap energy):

$$h\nu = E_0 - E_D - E_{A^*} + \frac{e^2}{4\pi\varepsilon_0\varepsilon_{\mathrm{st}}R_{\mathrm{DA}}}\ . \tag{5}$$

The last term of this equation takes into account the Coulomb energy of the electron and hole, where R_{DA} is the distance of donor and acceptor and ϵ_{st} is the static dielectric constant. An overlap of the wave functions can be neglected.[18] The Coulomb energy corresponds to the difference between the maximum of the DAP luminescence plus the donor binding energy and the free-

to-bound transitions of an electron from the conduction band to the acceptor ground state. The relaxation time of the acceptor (excited state to the ground state) is smaller than the recombination time of the DAP. Therefore, the recombination between donor ground state E_D and acceptor ground state E_A with recombination energy $h\nu'$ is observed:

$$h\nu' = E_0 - E_D - E_A + \frac{e^2}{4\pi\varepsilon_0\varepsilon_{st}R_{DA}} . \quad (6)$$

Thus, the difference of excitation and recombination energy is given by the formula

$$h\nu - h\nu' = E_{A^*} - E_A . \quad (7)$$

The resonant excitation energy for SPL transitions is similar to the recombination energy of acceptor bound excitons (as for THT transitions), since the binding energy of acceptor bound excitons (binding energy of free excitons,[19] 19.5 meV; binding energy of excitons at shallow acceptors[19] $\approx$ 10 meV) is similar to the donor binding energy. (Binding energy of the ground state for shallow donors $\approx$ 25 meV;[19,20] DA Coulomb energy; 5 – 10 meV, see Fig. 1.) Thus, SPL as well as THT's are excited with this resonant excitation energy and the difference between the well known excitation energy of the laser ($h\nu$) and the observed recombination energy ($h\nu'$) corresponds directly to the difference between the binding energy of the acceptor ground state and the excited acceptor states.

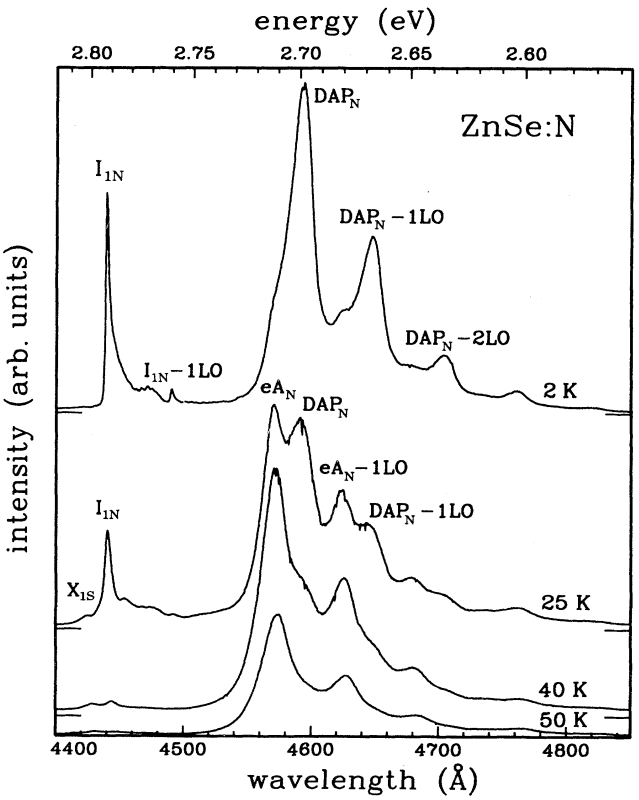

FIG. 1. Luminescence of a nitrogen-doped ZnSe sample prepared as a strain-free layer at different temperatures (thickness: 1 μm; interband excitation).

The investigations described in the following section were carried out on MBE- and MOVPE-grown samples. For both types of samples very similar results are obtained. For the resonant measurements presented in this work, we used MBE-grown ZnSe. The observation of excited acceptor states is more difficult for MOVPE than for MBE layers because of a higher impurity concentration in MOVPE-grown ZnSe. The impurities in undoped MOVPE ZnSe are mainly Cl donors, which are due to a pollution of the selenium sources. The identification of the impurities as Cl atoms will be published elsewhere.

The optimum dopant concentration for the observation of excited acceptor states by resonant PL methods is known to be 10^{15} – 10^{16} cm^{-3}. This concentration could easily be realized in our MBE- and MOVPE-grown samples.

A second DAP signal as described by several other authors[21–23] for highly nitrogen-doped ZnSe layers was not observed. Obviously for the nitrogen concentrations of our samples, nitrogen atoms are really incorporated as single acceptors and not as nitrogen-vacancy complexes.

IV. EXPERIMENTAL RESULTS

Figure 1 presents the luminescence spectra for interband excitation (excitation energy $\approx$ 3.5 eV) of a 1-μm-thick unstrained ZnSe:N layer at various temperatures. The investigations were carried out on a free-standing strain-free ZnSe layer in order to exclude strain effects caused by the substrate. In nitrogen-doped samples, a bound exciton luminescence I_{1N} at approximately 2.79 eV is observed, caused by excitons bound to neutral N acceptors. The spectra show an additional strong donor-acceptor-pair luminescence at 2.7 eV (DAP$_N$) with corresponding LO-phonon replica; for temperatures above 10 K, a free-exciton luminescence (X_{1S}) and free-to-bound transitions (eA_N) of electrons from the conduction band to the valence band appear.

The binding energy ($E_{1S_{3/2}}$) of the ground state for the nitrogen acceptor was determined by the difference between the recombination energy of free excitons [$E(X_{1S})$] and the free-to-bound transition [$E(eA)$] (binding energy of free excitons;[15,19] E_{BX} = 19.5 meV)

$$E_{1S_{3/2}} = E(X_{1S}) - E(eA) + E_{BX}. \quad (8)$$

The resulting energy obtained from Fig. 1 is given in Table I.

Excited acceptor states were investigated in this strain-free layer by THT's and SPL. In Fig. 2, THT/SPL spectra are shown for excitation energies varying from 2.7885 eV to 2.7927 eV. The energy scale represents the difference between the exciting photon energy of the laser line and the luminescence energy. Therefore, transitions with a constant difference to the excitation energy like THT, SPL, LO, and TO transitions appear in all spectra at the same position on this energy scale (as indicated by

TABLE I. Experimental $1S_{3/2}$ acceptor ground-state energies and excitation energies relative to $1S_{3/2}$ for different biaxial strains.

ϵ_{biax} (%)	$1S_{3/2}$ binding energy[a] (meV)	Excitation energies[b] (meV)					
		$1S^*_{3/2}$	$2P_{3/2}$	$2S_{3/2}$	$2S^*_{3/2}$	$2P_{5/2}(\Gamma_8)$	$3P_{3/2}$
0	110		67.7	79.6		82.6	90.1
0	110[c]		67.8[c]	79.9[c]		82.6[c]	89.8[c]
0.07	109	1.5		79.5	81.0		
−0.20	107	6.0		79.8	84.3		

[a]Accuracy ±1 meV.
[b]Accuracy ±0.2 meV, $1S^*_{3/2}$ ±0.5 meV.
[c]Ref. 24.

vertical dotted lines). However, transitions with recombination energies that are independent of the excitation energy like DAP recombinations have the tendency to shift from spectrum to spectrum to higher energies for increasing excitation energies. The symbols used for the excited acceptor states obey the notation of Baldereschi and Lipari.[4] The binding energies of the excited acceptor states can directly be obtained as the difference between the ground-state energy (110 meV) and the transition energies given in Table I, which are determined from Fig. 2. Table I also shows the experimental data of Shazad *et al.*,[24] which are in excellent agreement with our results.

The influence of strain on acceptor states was investigated for ZnSe/GaAs samples of different layer thicknesses between the critical thickness and 1 μm. The maximum of compressive strain is achieved for layer thicknesses that are smaller than the critical thickness: $\epsilon_{biax}(2\text{ K}) = -0.21\%$ (no strain relaxation during growth[15,16]), whereas the maximum of tensile strain is observed for a layer thickness of more than 1 μm: $\epsilon_{biax}(2\text{ K}) = +0.1\%$ (complete strain relaxation during growth[15,16]). The biaxial [001] strain reduces the crystal symmetry from T_d to D_{2d}. As a consequence, terms of symmetry $\Gamma_8(T_d)$ in the unstrained crystal (e. g., $nS_{3/2}$) split into $\Gamma_6(D_{2d})$ and $\Gamma_7(D_{2d})$ components.[25]

Figure 3 shows PL spectra at different temperatures for interband excitation of a nitrogen-doped ZnSe/GaAs layer with $\epsilon_{biax}(2\text{ K}) = -0.20\%$. The compressive strain causes a splitting of free excitons into a light-hole (X_l) and a heavy-hole (X_h) component and a shift of the

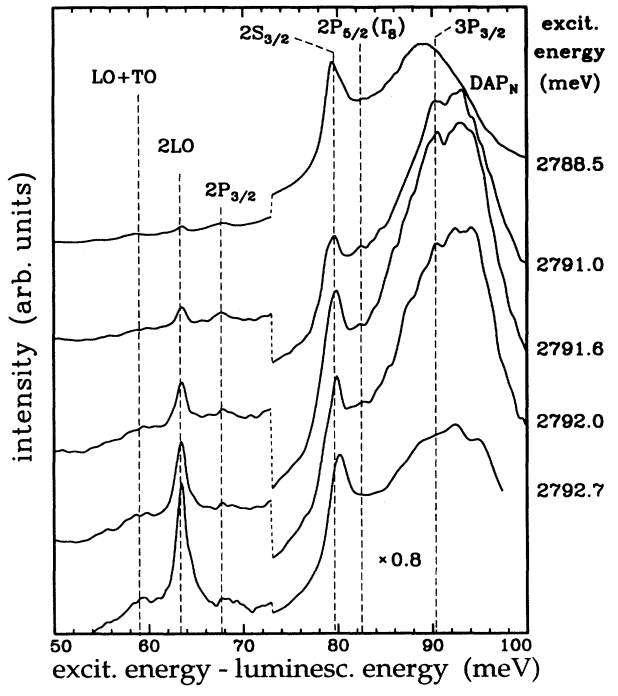

FIG. 2. SPL/THT spectra of a strain-free nitrogen-doped ZnSe layer at 2 K for different excitation energies. The spectra are plotted vs the difference between the excitation energy and the luminescence energy.

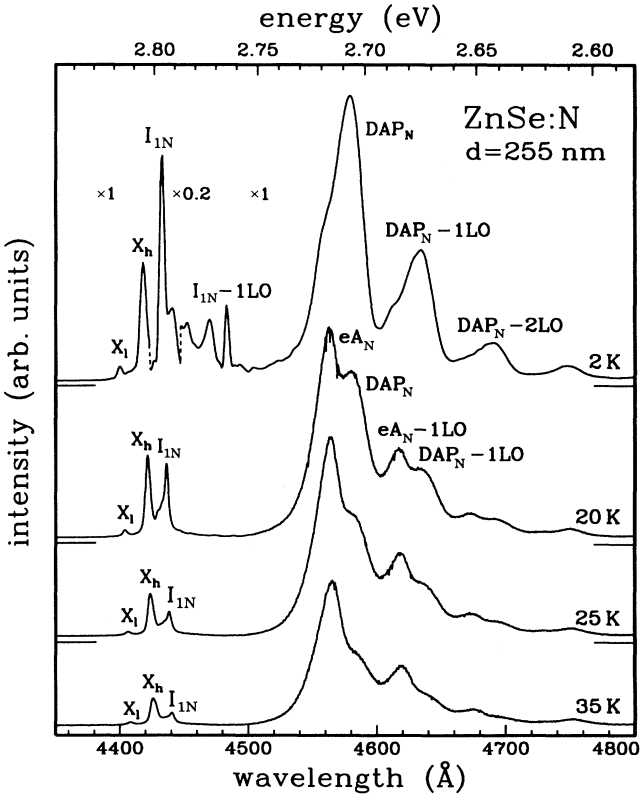

FIG. 3. Luminescence of a nitrogen-doped ZnSe/GaAs sample at different temperatures (thickness: 250 nm; interband excitation).

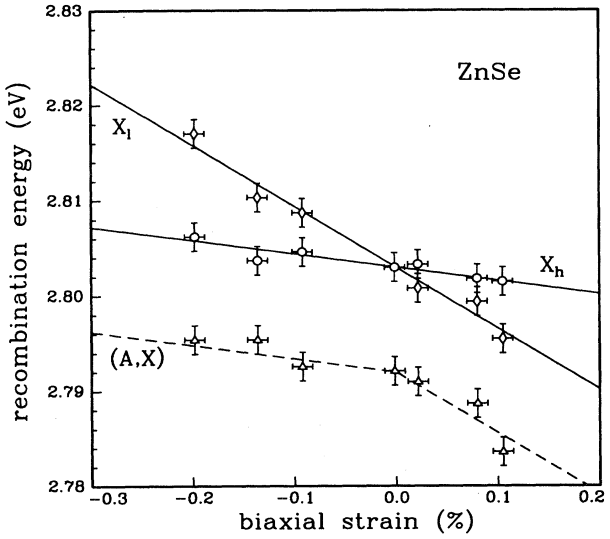

FIG. 4. Recombination energies of free heavy- and light-hole excitons (X_h and X_l) and of acceptor-bound excitons (A, X) for different compressive and tensile strain of ZnSe/GaAs layers (temperature 2 K, interband excitation). The lines are drawn to guide the eye.

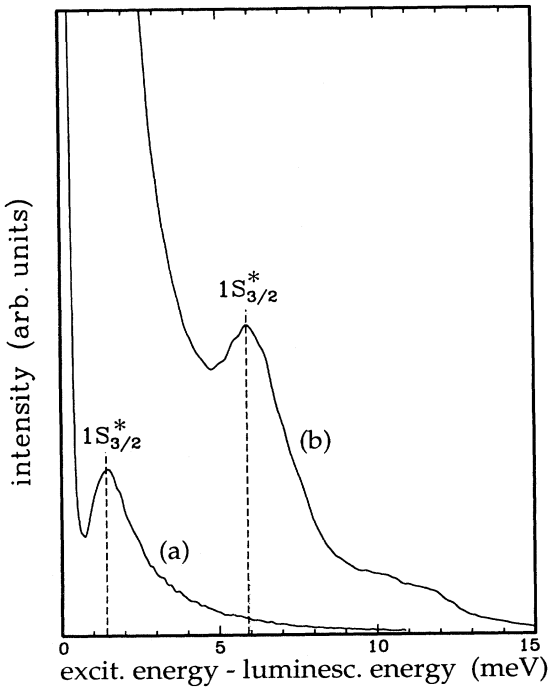

FIG. 5. THT spectra of nitrogen-doped ZnSe/GaAs layers at 2 K for (a) $\epsilon_{\text{biax}}(2\text{ K}) = +0.07\%$ (excitation energy = 2.790 eV), and (b) $\epsilon_{\text{biax}}(2\text{ K}) = -0.20\%$ (excitation energy = 2.797 eV). Acceptor-bound excitons are excited from the $1S_{3/2}$ ground state to the $1S^*_{3/2}$ excited state. The spectra are plotted vs the difference of the excitation energy and the luminescence energy.

whole spectra to higher energies compared to the unstrained layer. (Compare the recombination energy of bound excitons I_{1N}, DAP, and eA signals of Figs. 1 and 3.) The splitting of free excitons and the energy shift of free and acceptor-bound excitons were investigated for different layer thicknesses and strain conditions as shown in Fig. 4. For a change from compressive to tensile strain, the recombination energy of light-hole excitons decreases stronger than the recombination energy of heavy-hole excitons. Acceptor-bound excitons (A, X) behave similar to heavy-hole excitons for compressive strain and light-hole excitons for tensile strain. Obviously the trapping probability of free excitons to an acceptor is higher for the component with lower energy. Therefore, only one signal of acceptor-bound excitons is observed. Acceptor-bound excitons in tensile strained ZnTe/GaAs layers were identified by Wagner *et al.*[26] as light-hole excitons bound to neutral light-hole acceptors (A_l, X_l). From these investigations and the results of Fig. 4, it can be concluded that for tensile strained ZnSe/GaAs layers also light-hole excitons are bound to neutral light-hole acceptors, whereas for compressive strain, heavy-hole excitons are bound to neutral heavy-hole acceptors (A_h, X_h).

The $1S_{3/2}$ acceptor ground state observed in the unstrained crystal splits in strained layers into two components. The binding energy of the ground state was determined for two samples with $\epsilon_{\text{biax}}(2\text{ K}) = -0.20\%$ and $\epsilon_{\text{biax}}(2\text{ K}) = +0.07\%$. The values of the ground-state energies were determined from PL measurements (interband excitation) at temperatures above 10 K as presented in Fig. 3 and described above for an unstrained

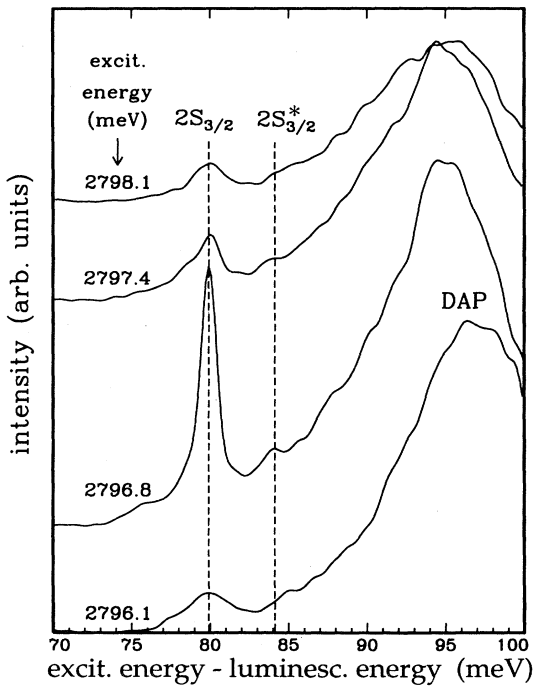

FIG. 6. SPL/THT spectra of a strained nitrogen-doped ZnSe/GaAs layer at 2 K [$\epsilon_{\text{biax}}(2\text{ K}) = -0.20\%$]. The spectra are plotted vs the difference of the excitation energy and the luminescence energy.

layer. The results are summarized in Table I. For these two samples, the energy difference between the ground state (labeled $1S_{3/2}$) and the split-off state (labeled $1S^*_{3/2}$) was investigated by resonant PL methods (Fig. 5). We selected the maximum of the I_{1N} peak [recombination energy of excitons bound to the acceptor ground state (A,X)] as excitation energy. In this case, a luminescence signal was observed a few meV lower than the photon energy of the laser light. This signal corresponds to the recombination energy of the excited (A^*,X) complex, whereas the excitation energy corresponds to the recombination energy of the (A,X) complex for the acceptor ground state. Therefore, the difference between the excitation energy and the maximum of the PL signal is identical with the energy difference of the $1S^*_{3/2}$ excited state and the $1S_{3/2}$ ground state of the acceptor. Thus, the binding energy of the excited state can be deduced from the binding energy of the ground state (see Table I).

The splitting of the $2S_{3/2}(\Gamma_8)$ state into a $2S_{3/2}$ and an energetically higher $2S^*_{3/2}$ component and the dependence of the binding energies on strain were also investigated for the two samples with $\epsilon_{\rm biax}(2\ {\rm K}) = -0.20\%$ and $\epsilon_{\rm biax}(2\ {\rm K}) = +0.07\%$. THT and SPL transitions were induced at 2 K by resonant PL measurements as described above for excited acceptor states of an unstrained layer. The spectra are presented in Figs. 6 and 7. The results of these experiments are also summarized in Table I.

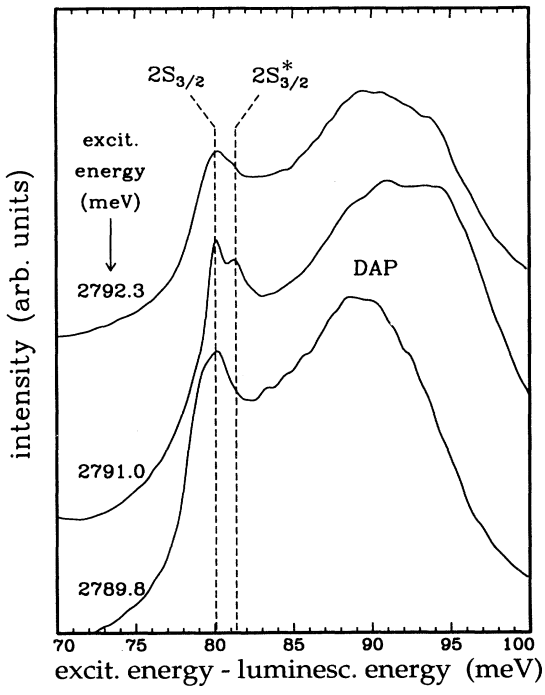

FIG. 7. SPL/THT spectra of a strained nitrogen-doped ZnSe/GaAs layer at 2 K [$\epsilon_{\rm biax}(2\ {\rm K}) = +0.07\%$]. The spectra are plotted vs the difference of the excitation energy and the luminescence energy.

V. THEORY

The $\mathbf{k}\cdot\mathbf{p}$ Hamiltonian for the acceptor in strained crystals consists of three parts:

$$H = H_{p^2} + H_\epsilon + V(r). \tag{9}$$

The kinetic energy H_{p^2} of the holes in the unstrained crystal is given by the Luttinger Hamiltonian, which describes the valence-band states in the vicinity of the fourfold degenerate Γ_8 valence-band edge:[3,4]

$$H_{p^2} = \frac{1}{2m_0}\left\{\gamma_1 p^2 - 2\gamma_2\left[(J_x^2 - \tfrac{1}{3}J^2)p_x^2 + \text{c.p.}\right] - 2\gamma_3\left[2\{J_yJ_z\}p_yp_z + \text{c.p.}\right]\right\}. \tag{10}$$

The Luttinger parameters γ_1, γ_2, and γ_3 weight the three possible irreducible tensor components bilinear in the components of the hole momentum. As essential details of the valence-band structure, this Hamiltonian contains the mass difference between heavy and light holes and the characteristic band warping, i.e., an anisotropy of the dispersion with cubic symmetry.

In the presence of axial strain, the valence-band edge splits into the heavy- and light-hole components. This splitting is linear in the axial strain and described by the Bir-Pikus Hamiltonian[7]

$$H_\epsilon = -D_d{\rm Tr}\,\epsilon - \tfrac{2}{3}D_u\left[(J_x^2 - \tfrac{1}{3}J^2)\epsilon_{xx} + \text{c.p.}\right] - \tfrac{2}{3}D'_u\left[2\{J_xJ_y\}\epsilon_{yz} + \text{c.p.}\right]. \tag{11}$$

Here ϵ_{ij} are the components of the strain tensor and D_d, D_u, and D'_u are deformation potentials. The effect of the hydrostatic component of the strain tensor is an overall energetic shift of the spectrum and may therefore be neglected in the calculation of single-particle energies. The parameters D_u and D'_u determine the valence-band splitting for axial $\langle 001\rangle$ and $\langle 111\rangle$ strain, respectively.

In the vicinity of the impurity site, the acceptor potential deviates from the pure Coulomb form. This leads to an impurity-specific shift of the ground-state energy, the so-called chemical shift of the different acceptor types in a given host crystal. We take this deviation into account by the empirical approach of Lipari, Baldereschi, and Thewalt,[8] which results in the potential[9]

$$V(r) = -\frac{e^2}{4\pi\varepsilon_0\varepsilon_{\rm st}r}\left[1 + (\varepsilon_{\rm st} - 1)e^{-\alpha' r}\right], \tag{12}$$

with the acceptor specific screening length α'^{-1}. It becomes effective for small r by reducing the screening and thus leads to a larger binding energy for even-parity states. Another modification of the Coulomb potential would result from the polar hole-phonon interaction. To our knowledge, this has not been considered so far together with the complex valence-band structure as a bound hole polaron. One would not expect, however, that this modification is sensitive to the strain. Therefore, we have not taken it into account.

Because a large portion of the acceptor Hamiltonian possesses spherical symmetry (or at least axial symmetry for the case of an axially strained crystal), it is conve-

nient to formulate the Hamiltonian in terms of spherical tensor components rather than in Cartesian components. This leads to the Hamiltonians given by Baldereschi and Lipari[4] for the unstrained crystal or by Pertzsch and Rössler[6] for the case of a strained crystal, respectively.

The acceptor Hamiltonian for [001] strain, written in terms of spherical tensor components $p_q^{(2)}$, $J_q^{(2)}$ reads

$$H_{p^2} = \frac{\gamma_1}{2m_0}\Big\{p^2 - \mu(p^{(2)}\cdot J^{(2)}) + \delta\big([p^{(2)}\times J^{(2)}]^{(4)}_{-4} + \sqrt{\tfrac{14}{5}}[p^{(2)}\times J^{(2)}]^{(4)}_{0} + [p^{(2)}\times J^{(2)}]^{(4)}_{4}\big)\Big\},$$
$$H_\epsilon = -D_d \operatorname{tr}\epsilon - \tfrac{2}{3}\sqrt{\tfrac{2}{3}}D_u(\epsilon_{zz}-\epsilon_{xx})J_0^{(2)}. \qquad (13)$$

The definition of the tensor products $[p^{(2)}\times J^{(2)}]^{(K)}_Q$ is given by Edmonds[27] and Pertzsch and Rössler.[6]

The parameters

$$\mu = \frac{6\gamma_3 + 4\gamma_2}{5\gamma_1}, \qquad \delta = \frac{\gamma_3-\gamma_2}{\gamma_1}, \qquad (14)$$

have been introduced by Baldereschi and Lipari.[4] The term weighted by μ couples the orbital motion to the hole spin, thus being analogous to the spin-orbit coupling in atomic physics, although it originates from the valence-band structure.

The Luttinger Hamiltonian consists of terms with spherical $[O(3)]$ and cubic (T_d) symmetry. The Bir-Pikus operator has axial symmetry $(D_{\infty h})$ with respect to the strain axis. Besides the simple hydrogenlike terms, the terms of lower symmetry contribute with two competing effects: (1) The coupling of hole spin $\mathbf{J}$ and orbital angular momentum $\mathbf{L}$ to the total angular momentum $\mathbf{F}=\mathbf{L}+\mathbf{J}$ with the resulting fine-structure splitting and (2) the strain-induced splitting into heavy-hole $(|J_z|=\frac{3}{2})$ and light-hole $(|J_z|=\frac{1}{2})$ states. The latter effect is usually the smaller one. This leads to a level scheme of strain-split fine-structure multiplets nL_F.

The symmetry of the complete Hamiltonian for axial [001] strain is D_{2d}. Thus, states of symmetry Γ_8 (T_d) split into two components of symmetry Γ_6 (D_{2d}) and Γ_7 (D_{2d}), respectively. (For the notation of irreducible representations of the point groups, see Koster *et al.*[25])

Eigenvalues of the Schrödinger equation

$$\{H_{p^2} + H_\epsilon + V(r)\}\,\Psi = E\Psi \qquad (15)$$

can be obtained by variational methods. In order to employ angular momentum techniques,[27] we expand the wave function, which transforms according to column λ of irreducible representation Γ_κ into products of symmetry-adapted linear combinations $\Upsilon^{(\kappa,\lambda)}(\theta,\phi)$ of angular momentum eigenfunctions $|L\tfrac{3}{2}FF_z\rangle$ and radial functions $f_i(r)$:

$$\Psi^{(\kappa,\lambda)}(\mathbf{r}) = \sum_i f_i(r)\Upsilon_i^{(\kappa,\lambda)}(\theta,\phi). \qquad (16)$$

The relevant angular functions $\Upsilon^{(\kappa,\lambda)}$ for D_{2d} symmetry are given in Table II. The spin-orbit term couples orbital angular momentum states with $\Delta L = 0,\pm 2$ and we are mainly interested in $1S$, $2S$, and $2P$ states; therefore, it is sufficient to consider states with $0 \le L \le 3$ in this expansion. Details of the variational procedure and our ansatz for the radial functions $f_i(r)$ have been published elsewhere.[28]

TABLE II. Symmetry-adapted linear combinations of the $|L\,\frac{3}{2}\,F\,F_z\rangle$ for D_{2d} symmetry.

i	$\Upsilon_i^{(6,-1/2)}$	$\Upsilon_i^{(7,-1/2)}$
1	$\lvert 0\,\frac{3}{2}\,\frac{3}{2}\,-\frac{1}{2}\rangle$	$\lvert 0\,\frac{3}{2}\,\frac{3}{2}\,\frac{1}{2}\rangle$
2	$\lvert 2\,\frac{3}{2}\,\frac{3}{2}\,-\frac{3}{2}\rangle$	$\lvert 2\,\frac{3}{2}\,\frac{3}{2}\,\frac{1}{2}\rangle$
3	$\lvert 2\,\frac{3}{2}\,\frac{5}{2}\,-\frac{3}{2}\rangle$	$\lvert 2\,\frac{3}{2}\,\frac{1}{2}\,\frac{1}{2}\rangle$
4	$\lvert 2\,\frac{3}{2}\,\frac{5}{2}\,\frac{5}{2}\rangle$	$\lvert 2\,\frac{3}{2}\,\frac{5}{2}\,\frac{1}{2}\rangle$
5	$\lvert 2\,\frac{3}{2}\,\frac{7}{2}\,-\frac{3}{2}\rangle$	$\lvert 2\,\frac{3}{2}\,\frac{7}{2}\,\frac{1}{2}\rangle$
6	$\lvert 2\,\frac{3}{2}\,\frac{7}{2}\,\frac{5}{2}\rangle$	$\lvert 2\,\frac{3}{2}\,\frac{7}{2}\,-\frac{7}{2}\rangle$
7	$\lvert 1\,\frac{3}{2}\,\frac{1}{2}\,\frac{1}{2}\rangle$	$\lvert 1\,\frac{3}{2}\,\frac{3}{2}\,-\frac{3}{2}\rangle$
8	$\lvert 1\,\frac{3}{2}\,\frac{3}{2}\,\frac{1}{2}\rangle$	$\lvert 3\,\frac{3}{2}\,\frac{3}{2}\,-\frac{3}{2}\rangle$
9	$\lvert 3\,\frac{3}{2}\,\frac{3}{2}\,\frac{1}{2}\rangle$	$\lvert 1\,\frac{3}{2}\,\frac{5}{2}\,-\frac{5}{2}\rangle$
10	$\lvert 1\,\frac{3}{2}\,\frac{5}{2}\,\frac{1}{2}\rangle$	$\lvert 3\,\frac{3}{2}\,\frac{5}{2}\,-\frac{5}{2}\rangle$
11	$\lvert 3\,\frac{3}{2}\,\frac{5}{2}\,\frac{1}{2}\rangle$	$\lvert 1\,\frac{3}{2}\,\frac{5}{2}\,\frac{5}{2}\rangle$
12	$\lvert 3\,\frac{3}{2}\,\frac{7}{2}\,\frac{1}{2}\rangle$	$\lvert 3\,\frac{3}{2}\,\frac{5}{2}\,\frac{5}{2}\rangle$
13	$\lvert 3\,\frac{3}{2}\,\frac{9}{2}\,\frac{1}{2}\rangle$	$\lvert 3\,\frac{3}{2}\,\frac{7}{2}\,-\frac{3}{2}\rangle$
14	$\lvert 3\,\frac{3}{2}\,\frac{7}{2}\,-\frac{7}{2}\rangle$	$\lvert 3\,\frac{3}{2}\,\frac{7}{2}\,-\frac{7}{2}\rangle$
15	$\lvert 3\,\frac{3}{2}\,\frac{9}{2}\,-\frac{7}{2}\rangle$	$\lvert 3\,\frac{3}{2}\,\frac{9}{2}\,-\frac{3}{2}\rangle$
16	$\lvert 3\,\frac{3}{2}\,\frac{9}{2}\,\frac{9}{2}\rangle$	$\lvert 3\,\frac{3}{2}\,\frac{9}{2}\,\frac{5}{2}\rangle$

VI. DISCUSSION

When applied to unstrained layers, the model outlined in the previous section contains five material-specific parameters: the Luttinger parameters γ_1, γ_2, and γ_3, the static dielectric constant $\varepsilon_{\rm st}$, and the screening length of the central-cell correction α'^{-1}. Throughout all of our calculations, we used the value $\varepsilon_{\rm st} = 9.1$, taken from the Landoldt-Börnstein tables.[29] In contrast to other standard semiconductors, there seems to be no well-established set of valence-band effective mass parameters for ZnSe. For example, values of γ_1 have been reported in the past in the range between 2.45 (Ref. 30) and 4.3 (Refs. 31 and 32). In principle, the experimental acceptor data obtained in the present experiment could be used to determine these parameters by fitting the calculated binding energies. For such a procedure, experimental data for the $nS_{3/2}$ states cannot be used, due to their strong dependence of the *a priori* unkown central-cell correction. As far as the nP_F states are concerned, one has to bear in mind that their absolute binding energy is known only with the accuracy of the acceptor ground-state energy, i. e., ± 1 meV. Within this accuracy, a fitting procedure employed for different values of γ_1 showed that reasonable agreement between calculated and experimental binding energies of the nP_F states can be achieved for any value of γ_1 in the range cited above. An increase in γ_1 leading to a reduction of the effective Rydberg energy can always be compensated by choosing a larger value of μ (see Fig. 8). Consequently a larger value of γ_1 results in larger values for γ_2 and γ_3.

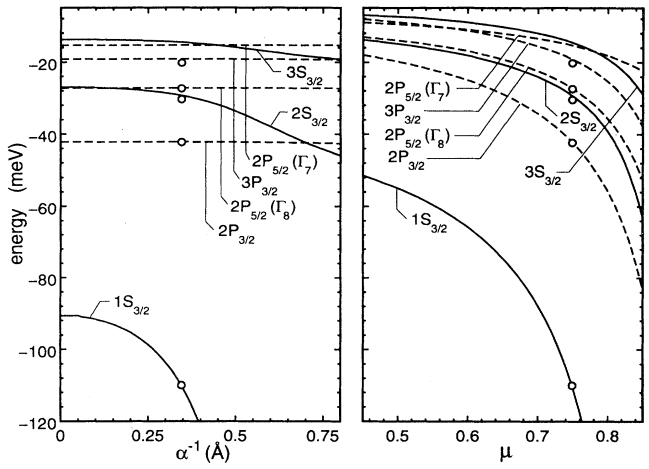

FIG. 8. Nitrogen acceptor levels in unstrained ZnSe as a function of (a) the screening length α'^{-1} and (b) the spin-orbit parameter μ. ○, experimental data: solid lines, even-parity states: dashed lines, odd-parity states. All other parameters are fixed at the fitted values.

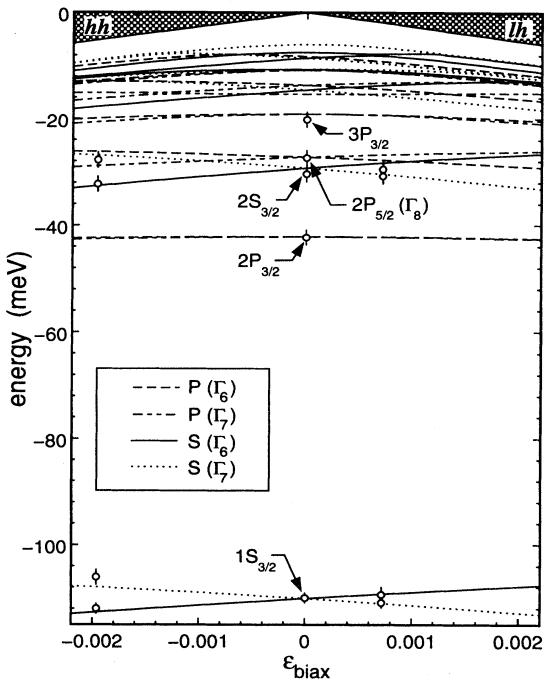

FIG. 9. Strain dependence of the nitrogen acceptor levels in ZnSe for [001] biaxial strain. Solid line, $S(\Gamma_6)$ states: dotted line, $S(\Gamma_7)$ states: dashed line, $P(\Gamma_6)$ states: dash-dotted lines, $P(\Gamma_7)$ states: ○, experimental data.

If the strain dependence of the $nS_{3/2}$ states is included, which will be discussed below, the value of $\gamma_1 = 4.3$ appears to be favorable. This value has previously been determined by Feierabend and Weber,[33] Venghaus,[31] and Sermage and Fishman[32] using exciton data and an electron mass of $m^* = 0.16m_0$. With γ_1 fixed at this value, the fitting procedure yields parameters $\mu = 0.75$ and $\delta = 0.22$. These correspond to Luttinger parameters $\gamma_2 = 1.04$ and $\gamma_3 = 2.00$, which are in excellent agreement with those of Sermage and Fishman[32] ($\gamma_2 = 1.14$ and $\gamma_3 = 1.84$). The latter values have also been used successfully for the description of resonant Brillouin scattering data in biaxially strained ZnSe.[17]

Finally, we determined the screening length $\alpha'^{-1} = 0.35$ Å for the nitrogen acceptor in ZnSe by a fit to the experimentally observed $1S_{3/2}$ and $2S_{3/2}$ binding energies in unstrained material. Figure 8 shows details of the fitting procedure for two directions in parameter space. It is interesting to note, that for our parameter set the third-lowest odd-parity state has to be assigned to the $3P_{3/2}$ term and not to $2P_{5/2}(\Gamma_7)$. This is due to the relatively large value of the hole spin-orbit coupling parameter $\mu = 0.75$. Unfortunately, the often-used tables of Baldereschi and Lipari[4] lack information about this level. Therefore, Shazad *et al.*[24] have not been aware of the possibility to find the $3P_{3/2}$ state in their spectra and assigned the resonance to $2P_{5/2}(\Gamma_7)$. However, our calculations demonstrate that for sufficiently large μ, $3P_{3/2}$ has a larger binding energy than $2P_{5/2}(\Gamma_7)$.

For our calculations of the strain dependence, we used the deformation potential[34] $D_u = 1.7$ eV and the compliance constants[35] $s_{11} = 0.226 \times 10^{-10}$ Pa^{-1} and $s_{12} = -0.085 \times 10^{-10}$ Pa^{-1}. The resulting binding energies are shown in Fig. 9 as functions of biaxial strain. A continuum of unbound states appears for tensile biaxial strain above the light-hole band edge, for compressive strain above the heavy-hole band edge, respectively. These parts of the spectrum are indicated by the shaded areas. The continuum edge represents the reference point for the experimentally observed binding energies. The latter are displayed for comparison with the theoretical results. For vanishing strain, the labeling of the states follows that of Baldereschi and Lipari whereas in the presence of biaxial strain the states are classified by their symmetry with respect to the underlying point group D_{2d} and their parity.

Our calculation yields a very similar splitting of the $1S_{3/2}$ and $2S_{3/2}$ terms, which is in good agreement with the experimental results. For compressive biaxial strain, the $nS_{3/2}$ states can be assigned to $S(\Gamma_6)$ terms, the $nS^*_{3/2}$ states to $S(\Gamma_7)$ terms. For tensile strain, the symmetry classification is just switched: the $nS_{3/2}$ states can be identified as $S(\Gamma_7)$ terms, whereas the $nS^*_{3/2}$ states have $S(\Gamma_6)$ symmetry. The splitting of the $2P_{5/2}(\Gamma_8)$ term is significantly smaller, and the $nP_{3/2}$ terms show almost no splitting. All strain splittings are smaller than those of the valence-band edge. This is due to the fact that the spin-orbit term and the cubic correction induce a mixing of heavy- and light-hole states. Unfortunately no experimental data about the strain splitting of odd-parity $nP(\Gamma_8)$ acceptor states are available.

In conclusion, we performed a systematic experimental and theoretical investigation of the strain splitting of nitrogen acceptor levels in ZnSe. Both the splittings of the $1S_{3/2}$ ground state and the $2S_{3/2}$ excited state are in good agreement with theoretical calculations, which are

based on the $\mathbf{k} \cdot \mathbf{p}$ description of the acceptor problem. The strain splitting of all acceptor levels is reduced compared to the splitting of the valence-band edge, which is due to generic band-structure effects. The magnitude of the observed splittings demonstrates the necessity to take into account the strain effects when analyzing acceptor data obtained from strained layers.

ACKNOWLEDGMENTS

We gratefully acknowledge financial support by the Bundesministerium für Forschung und Technologie and by the Deutsche Forschungsgemeinschaft–Schwerpunktprogramm II-VI-Halbleiter and Graduiertenkolleg: "Komplexität in Festkörpern."

[1] M. Haase, J. Qiu, J. DePuydt, and H. Cheng, Appl. Phys. Lett. **59**, 1272 (1991).
[2] H. Jeon, W. Patterson, A. V. Nurmikko, W. Xie, D. C. Grillo, M. Kobayashi, and R. L. Gunshor, Appl. Phys. Lett. **59**, 3619 (1991).
[3] J. M. Luttinger and W. Kohn, Phys. Rev. **97**, 869 (1955); J. M. Luttinger, *ibid.* **102**, 1030 (1956).
[4] A. Baldereschi and N. C. Lipari, Phys. Rev. B **8**, 2697 (1973); **9**, 1525 (1974).
[5] R. Buczko, Nuovo Cimento **9**, 669 (1987).
[6] B. Pertzsch and U. Rössler, Phys. Status Solidi B **89**, 475 (1978).
[7] G. L. Bir and G. E. Pikus, *Symmetry and Strain-Induced Effects in Semiconductors* (Wiley, New York, 1972).
[8] N. O. Lipari, A. Baldereschi, and M. L. W. Thewalt, Solid State Commun. **33**, 277 (1980).
[9] M. A. Kanehisa and M. Said, J. Phys. C **21**, 4637 (1988).
[10] H. Stanzl, K. Wolf, S. Bauer, W. Kuhn, A. Naumov, and W. Gebhardt, J. Electron. Mater. **22**, 501 (1993).
[11] K. Wolf, H. Stanzl, A. Naumov, H. P. Wagner, W. Kuhn, B. Hahn, and W. Gebhardt, J. Cryst. Growth **138**, 412 (1994).
[12] A. Rosenauer, T. Reisinger, E. Steinkirchner, J. Zweck, and W. Gebhardt, J. Cryst. Growth **152**, 42 (1995).
[13] H. Leiderer, A. Supritz, M. Silberbauer, M. Lindner, W. Kuhn, H. P. Wagner, and W. Gebhardt, Semicond. Sci. Technol. **6**, A101 (1991).
[14] W. J. Bartels, J. Vac. Sci. Technol. B **21**, 338 (1983).
[15] K. Wolf, Ph.D. thesis, Universität Regensburg, 1994.
[16] K. Wolf, S. Jilka, A. Rosenauer, G. Schütz, H. Stanzl, T. Reisinger, and W. Gebhardt, in Proceedings of 2nd European Symposium on X-Ray Topography and High Resolution Diffraction, Berlin 1994 [Appl. Phys. **28**, A120 (1995)].
[17] H. Mayer, U. Rössler, S. Permogorov, H. Stolz, H. Vogelsang, and W. von der Osten, J. Cryst. Growth **138**, 195 (1994).
[18] A. T. Vink, R. L. A. van der Heyden, and J. A. W. van der Does de Bye, J. Lumin. **8**, 105 (1973).
[19] J. Gutwoski, N. Presser, and G. Kudlek, Phys. Status Solidi A **120**, 11 (1990).
[20] F. E. Williams, Phys. Status Solidi B **25**, 493 (1968).
[21] J. Simpson, I. Hauksson, S. Y. Wang, H. Stewart, K. A. Prior, and B. C. Cavenett, Physica B **185**, 164 (1993).
[22] I. Hauksson, J. Simpson, S. Y. Wang, K. A. Prior, and B. C. Cavenett, Appl. Phys. Lett. **61**, 2208 (1992).
[23] Z. Zhu, K. Takebayashi, K. Tanaka, T. Ebisutani, J. Kawamata, and T. Yao, Appl. Phys. Lett. **64**, 91 (1994).
[24] K. Shazad, B. A. Kahn, D. J. Olego, and D. A. Cammack, Phys. Rev. B **42**, 11 240 (1990).
[25] G. F. Koster, J. O. Dimmock, R. G. Wheeler, and H. Statz, *Properties of the Thirty-Two Point Groups* (MIT Press, Cambridge, MA, 1963).
[26] H. P. Wagner, S. Lankes, K. Wolf, D. Lichtenberger, W. Kuhn, P. Link, and W. Gebhardt, J. Lumin. **52**, 41 (1992).
[27] A. R. Edmonds, *Angular Momentum in Quantum Physics* (Princeton University Press, Princeton, NJ, 1960).
[28] H. Mayer, M. Steckermeier, and U. Rössler, Philos. Mag. B **70**, 335 (1994).
[29] *Physics of II-VI and I-VII Compounds*, edited by Ö. Madelung, Landolt-Börnstein, New Series, Group III, Vol. 17, Pt. b (Springer, Berlin, 1982); *Intrinsic Properties of Group IV Elements and III-V, II-VI and I-VII Compounds*, edited by Ö. Madelung, Landolt-Bornstein, New Series, Group III, Pt. a (Springer, Berlin, 1987).
[30] H. W. Hölscher, A. Nöthe, and Ch. Uihlein, Phys. Rev. B **31**, 2379 (1985).
[31] H. Venghaus, Phys. Rev. B **19**, 3071 (1979).
[32] B. Sermage and G. Fishman, Phys. Rev. B **23**, 5107 (1981).
[33] S. Feierabend and H. G. Weber, Solid State Commun. **26**, 191 (1978).
[34] B. Rockwell, H. R. Chandrasekhar, and M. Chandrasekhar, Phys. Rev. B **44**, 20 (1991).
[35] D. Berlincourt, H. Jaffe, and L. R. Shiozawa, Phys. Rev. **129**, 1009 (1963).